Journal of Glaciology

Article

Cite this article: Dey R, Thamban M, Laluraj CM, Mahalinganathan K, Redkar BL, Kumar S, Matsuoka K (2023). Application of visual stratigraphy from line-scan images to constrain chronology and melt features of a firn core from coastal Antarctica. *Journal of Glaciology* **69**(273), 179–190. https://doi.org/10.1017/jog.2022.59

Received: 27 August 2021
Revised: 14 June 2022
Accepted: 15 June 2022
First published online: 19 July 2022

Key words:
Antarctica; chronology; firn; melt layer; visual stratigraphy

Author for correspondence:
Rahul Dey,
E-mail: rdey1801@gmail.com,
rahuldey@ncpor.res.in

cambridge.org/jog

Application of visual stratigraphy from line-scan images to constrain chronology and melt features of a firn core from coastal Antarctica

Rahul Dey[1,2], Meloth Thamban[1], Chavarukonam Madhavanpillai Laluraj[1], Kanthanathan Mahalinganathan[1], Bhikaji Laxman Redkar[1], Sudhir Kumar[3] and Kenichi Matsuoka[4]

[1]National Centre for Polar and Ocean Research (NCPOR), Ministry of Earth Sciences, Vasco-da Gama, Goa 403804, India; [2]School of Earth, Ocean and Atmospheric Sciences (SEOAS), Goa University, Goa 403206, India; [3]Hydrological Investigations Division, National Institute of Hydrology, Ministry of Jal Shakti, Roorkee 247667, India and [4]Norwegian Polar Institute, Framsentret, Postboks 6606, Langnes, 9296 Tromsø, Norway

Abstract

Establishing an accurate chronology is crucial for interpretation of ice core-based climatic records. While high snow accumulation rates characterise coastal Antarctica, thus enabling recovery of highly resolved climatic records, summertime melting at such low-elevation sites offers challenges in establishing a reliable chronological framework through traditional approaches using the seasonality of stable water isotope and ionic proxy records. Here, we assess visual stratigraphy (VS) obtained from line-scan images as a proxy for annual layer counting in firn section (top 50 m) of the IND-36/B9 ice core (dated 1919–2016 CE) from the Djupranen Ice Rise in central Dronning Maud Land, East Antarctica. We also used these images to obtain melt history for the site and found that traditional thickness-based quantification of melt proportion results in significant overestimations. Since density has dominant control on VS profile over the firn section, we first used circulant single-spectrum analysis to remove the secular trend and then we extracted the seasonal VS signals attributed to dust and sea-salt inclusions. We find that melt layers do not significantly alter the VS records if masked during pre-processing. The age–depth model based on the reconstructed VS profile revealed an excellent match with identified time-markers within an uncertainty of ±2 years.

1. Introduction

Polar ice cores can provide annually resolved proxy records of past atmospheric temperature, composition and circulation changes for thousands of years when instrumental records are not available. Ice core studies have enabled us to better understand human-induced warming on a global scale and the non-linear behaviour of the climate system at multiple timescales. However, the reliability of any palaeoclimate data is most dependent on the accuracy of its chronology and constructing a robust age model is essential for interpreting past climatic records from polar ice cores (Legrand and Mayewski, 1997; Sinclair and others, 2010). Considering the large spatial variability in Antarctic snowfall, the local estimation of snow accumulation rate is vital for estimates of the coastal Antarctic mass balance (Krinner and others, 2007), assessments of regional climate models, validations of satellite measurements (Stenni and others, 2000; Goursaud and others, 2017) and eventually deciphering interactions between the Antarctic ice sheet, atmosphere and ocean (Stenni and others, 2000; Sinclair and others, 2010).

Multiple and complementary methods are often used to establish more reliable ice core chronologies. When chronology for the past few centuries is established in coastal Antarctica, these methods are mainly a combination of annual layer counting, use of time markers and correlation with other dated time series, occasionally complemented with glaciological modelling (Stenni and others, 1999; Zhang and others, 2006; Thamban and others, 2013). High snow accumulation sites in the coastal region offer excellent opportunities to reconstruct sub-annual to annual climatic records by counting annual layers of stable water isotopes (Naik and others, 2010; Thamban and others, 2013; Philippe and others, 2016). However, there are many complicating factors like the damping effect due to diffusion processes during firnification, especially where the snow accumulation rate is lower than 0.2 m w.e. (Johnsen, 1977). More importantly, summer surface melting in coastal Antarctica can induce post-depositional effects in the stable isotope records. Therefore, a multiproxy approach is preferred for dating an ice core, generally using a combination of stable isotopes and chemistry records. Such an approach has limitations for coastal sites, which are influenced by storm activities and summertime melting, making the annual layer counting using stable isotope and chemistry records very complicated.

Visual stratigraphy (VS) obtained by line-scan imaging is commonly acquired information in many ice core studies. Light scattering is caused by micro-inclusions, such as solid

particulate matter and firn structure (or air bubbles enclosed in the ice matrix at greater depths), and its characteristics depend on the size and concentration of these inclusions, which may change with the seasons, resulting in dark and bright bands. The VS can be acquired using many techniques ranging from simple ocular inspection to digital scanning at high resolution, using a variety of different light sources (Kameda and others, 1995; Alley and others, 1997; Pohjola and others, 2002; Takata and others, 2004; Svensson and others, 2005; McGwire and others, 2008; Abram and others, 2013; Morcillo and others, 2020). The high-resolution images obtained using digital scanning can differentiate the annual layers even at depths below the bubble hydrate transition zone (Svensson and others, 2005; Svensson and others, 2008; Winstrup and others, 2012). Although VS has been extensively studied in ice cores from the Arctic and a few inland sites of Antarctica, studies from coastal Antarctica are limited. No studies have utilised VS as a proxy for annual layer counting of the firn section of ice cores from coastal Antarctica, where the climatic variability is higher due to the maritime influence and frequent episodes of extreme precipitation events, which in turn results in noise in the proxy records. These sites are also characterised by high-accumulation rates and occasional to frequent melt features, which add complexities to the VS record, making it harder to obtain a clear annual signal. While micro-inclusions are the significant source of variability within VS data in deeper core sections, gradual densification processes and summer melting also contribute to VS data changes in the upper firn sections (Sjögren and others, 2007; Kinnard and others, 2008). Summer melting is significant in the coastal regions of Antarctica (Das and Alley, 2005; van den Broeke, 2005; Kaczmarska and others, 2006; Tedesco and Monaghan, 2009; Lenaerts and others, 2017). Although there are several uncertainties related to the transport and refreezing of meltwater within the snowpack, the refrozen ice can be easily differentiated from the surrounding firn and ice in the VS profiles as they appear as dark and transparent layers with few or no bubbles. While surface melting is affected by numerous factors like surface albedo and cloud type, summer temperature is the primary factor responsible for melting the glacial surface (Winski and others, 2018). Melt layers in ice cores provide a valuable record of the summertime warming trend over recent times (Kaczmarska and others, 2006; Kelsey and others, 2010). Thus, a record of melt history from a coastal site can be a proxy for summer temperature trends in the past and complement surface air temperature reconstructions using water-stable isotopes. In this study, we examined VS profiles of a high-accumulation firn core from coastal Dronning Maud Land (DML) to assess the suitability of VS method for annual layer counting in the snow and firn sections of coastal Antarctic ice cores.

2. Materials and methods

2.1 Ice core

A new 122 m long firn core IND-36/B9 (hereafter IND36/9) was retrieved during the 2016–17 austral summer from the summit of the Djupranen Ice Rise (70.18° S, 9.18° E; elevation 321 m a.s.l.), at the western margin of the Nivlisen Ice Shelf, the central DML coast in East Antarctica (Fig. 1). The DML coast is characterised by distinct topographic features like ice rises having their specific local flow, climate regime and surface mass-balance variability (Lenaerts and others, 2014; Drews and others, 2015; Matsuoka and others, 2015; Goel and others, 2017; Rignot and others, 2019; Pratap and others, 2021). The coastal DML also offers opportunities for reconstructing annually resolved decadal to multi-decadal variability in temperature, westerly winds, sea ice and their interactions with various regional climatic modes (Naik and others, 2010; Philippe and others, 2016; Goel and others, 2020; Laluraj and others, 2020; Thamban and others, 2020; Ejaz and others, 2021; Pratap and others, 2021).

2.2 Ice core processing and line scanning

For this study, we used the top 50 m of the firn section of the IND36/9 ice core. The ice core was cut into 3.5 cm thick, 10 cm wide slabs for line scanning. Both sides of these slabs were polished using a pre-cleaned handheld microtome blade to remove surface undulations resulting from cutting the ice slab using a bandsaw. The VS measurements were done using an intermediate layer core scanner (ILCS), which was designed to perform a transect of a planar ice core at a predetermined depth, providing an intermediate layer scan of the ice core (Krischke and others, 2015). The ILCS works on the principle of dark field microscopy with two LED line illumination sources of wavelength 640 ± 20 nm. Dark field is a method of illuminating a sample with an oblique light source, so the camera only records the light scattered through the sample. The direct light from the light source falls outside the camera's field of view and therefore does not appear in the image, thus resulting in a dark, almost black background with bright objects. The two illumination sources are placed below the polished ice core slab at an incident angle of 45°, and the camera is placed above the sample to measure obliquely forward scattering (Fig. 2). Areas of the ice core with a high concentration of micro-inclusions will scatter more light and be recorded as bright bands, whereas areas of clear ice like melt layers appear dark. While the core sample was fixed, the 2048-pixel monochrome 8-bit line-scan camera and light sources were moved synchronously along the ice core using a computer-controlled motorised unit. The maximum scan length is 1200 mm with a single scan and 1700 mm with two overlapping scans, having a scan width of 105 mm and an effective resolution of 51 µm pixel^{-1}. The length of the overlapping scans is restricted to the length of the ice core tray (1750 mm). The image data are transferred via a Gigabit Ethernet interface to SKan-G-ILCS software used for image acquisition and inspection (Krischke and others, 2015). The top 1.67 m of the core is composed of low-density firn and was too fragile to fit into the core tray and was therefore not scanned. After line scanning, the ice slabs were cut at 5 cm resolution for stable isotope and chemical analysis. The samples for chemical analysis were cut into cuboids; the three dimensions of the samples were measured using a calliper and weighed using a weighing balance. The density for the samples was calculated as mass divided by the volume of each sample. The error in measuring the sample dimensions was ±0.5 mm, while the weighing balance's uncertainty was ±0.1 g for measurements up to 100 g. As a result, the density measurements have a propagated uncertainty of 5%.

2.3 Image processing

The monochrome line-scan camera records 8-bit greyscale images of the ice core section (Fig. 3a). The intensity of the scattered light, recorded as pixel intensity values with the 8-bit resolution, ranges from 0 (black) to 255 (white, saturated). Theoretically, the pixel intensity value of a section of clear ice should be zero, which is rarely observed in our study. All image processing was done using MATLAB (version 2018a, The MathWorks, Inc., Natick, Massachusetts, United States), as summarised below. To remove the image section outside the core sample, we first assign a value of 255 to pixels with a value greater than half of the mean value of all pixels in the image (Fig. 3b). A 7 × 7 structural element was then used to erode and then subsequently dilate the greyscale image morphologically. This greyscale image was then

https://doi.org/10.1017/jog.2022.59 Published online by Cambridge University Press

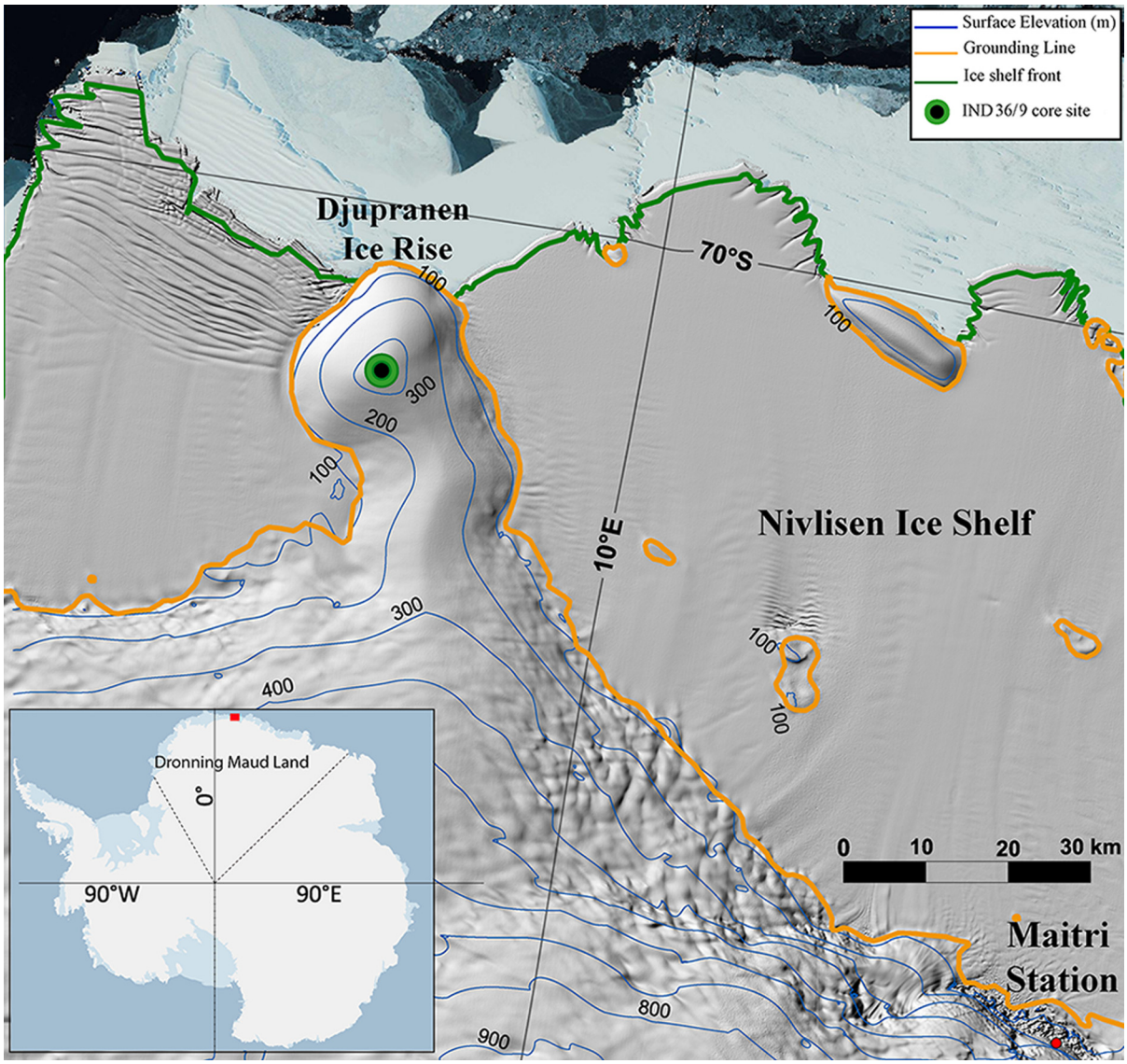

Fig. 1. Regional settings of the IND36/9 core site (green circle) at the summit of the Djupranen Ice Rise in coastal DML. The background image is a hillshade extracted from the Reference Elevation Model of Antarctica (Howat and others, 2019), with grounding line (Mouginot and others, 2017) and ice shelf fronts digitised from Radarsat-2 imagery taken between 2012 and 2014 (Goel and others, 2020). This map was made using Quantarctica (Matsuoka and others, 2021).

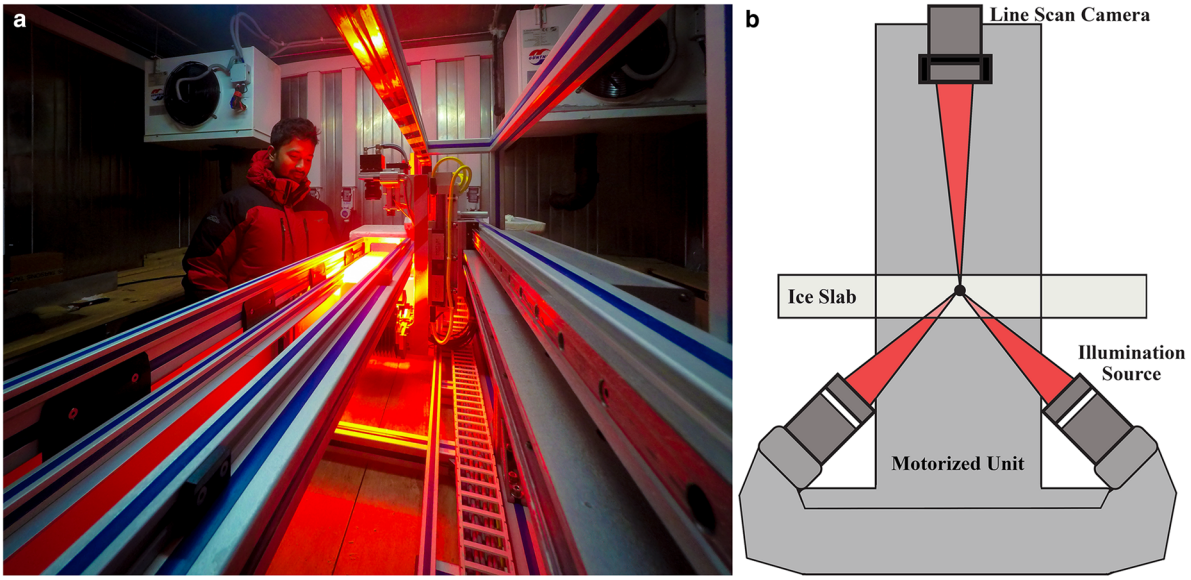

Fig. 2. (a) ILCS line-scanning set up at the Ice Core Lab of the National Centre for Polar and Ocean Research. The bright object in front of the person is the ice core being scanned. (b) Schematic cross-sectional representation of ILCS imaging technique. The line-scan camera above the ice slab moves synchronously (perpendicular to the page) with the two line-LED illumination sources mounted below the slab at an incident angle of 45°.

https://doi.org/10.1017/jog.2022.59 Published online by Cambridge University Press

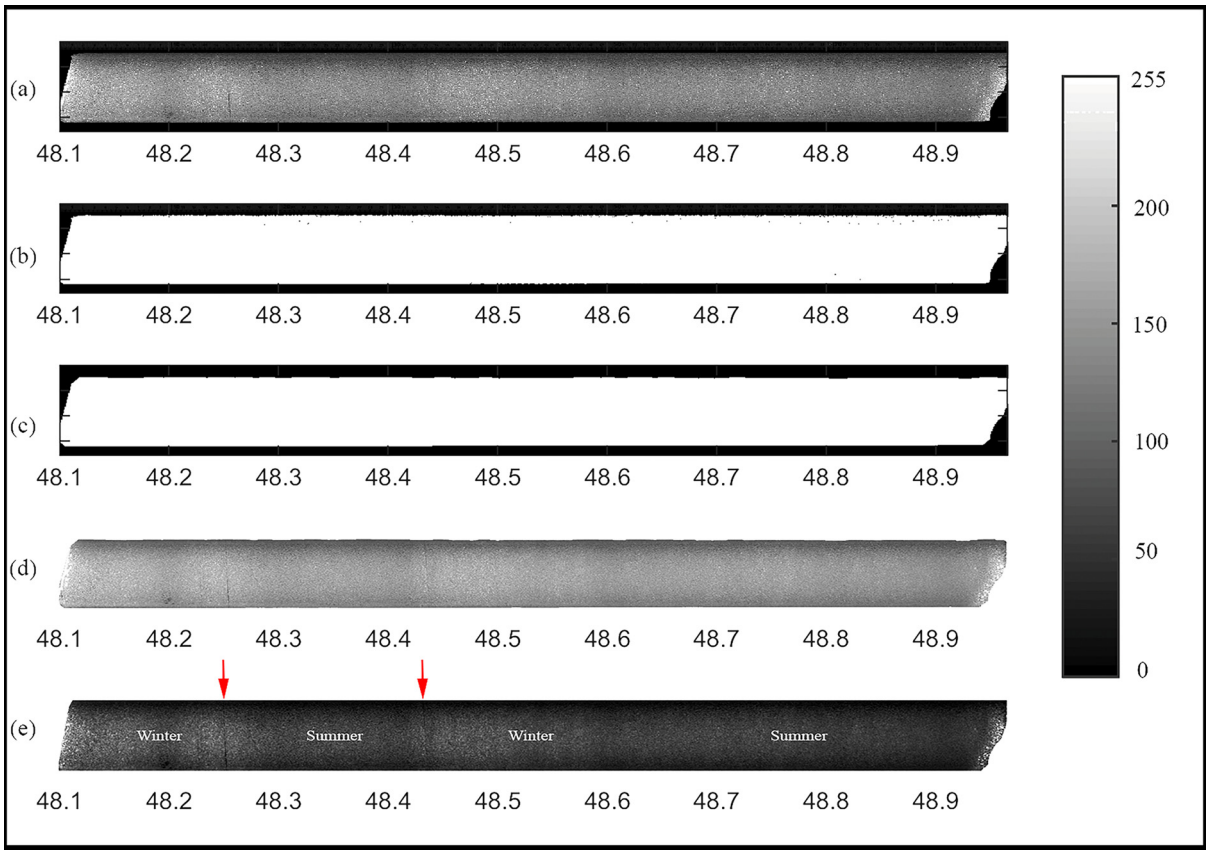

Fig. 3. Line-scan image processing steps from the raw image (a) to the final image (e) are presented for a core sample from 48.1 to 48.97 m depth. The contrast of the final image is exaggerated to make the annual layer visible, and the approximate seasonal positions are labelled. The core section is 87 cm long and 10 cm wide. The identical greyscale is used for all panels. See text for image processing procedures corresponding to individual panels. Two minor melt layers are identified in (e) and indicated with red arrows.

converted to a binary image, and the holes were flood-filled. A 250-pixel disc structuring element was then used to erode morphologically and then dilate the binary image to remove any objects smaller than 250 pixels in width, resulting in a mask of the ice core section (Fig. 3c). Finally, the central 7 cm wide section of the sample object was extracted (Fig. 3d). The image contrast was enhanced using contrast-limited adaptive histogram equalisation (CLAHE) with exponential distribution (Fig. 3e). The CLAHE is a variant of adaptive histogram equalisation in which contrast amplification is limited to reduce problems of noise amplification (Magudeeswaran and Singh, 2017). Breaks in the ice core sometimes appear as saturated pixels, and these regions were excluded from further analysis. A total of 1.5% of the total ice core length was thus excluded. We used the arithmetic mean of grey values along the width of the core sections as a parameter for further analysis.

A continuous VS profile was merged for the 50 m length of the ice core. Considering the sub-millimetre-scale (51 μm pixel^{-1}) scanning of ILCS, the VS profiles have the potential to provide an extremely detailed record of snow accumulation and sea-salt inclusions. Due to the inherent noise involved in such ultra-high-resolution data of line scanning and to make it comparable with the $\delta^{18}O$ records, the VS profiles were downsampled at 5 cm resolution by calculating the mean of greyscale values for every 5 cm intervals at which discrete isotopic and chemical analysis were performed. This enabled us to enhance the signal-to-noise ratio and improve confidence in annual layer counting.

3. Results and discussion

3.1 Preliminary chronology and age constraints

A preliminary chronology for the IND36/9 ice core was developed using annual layer counting of the $\delta^{18}O$ record, using winter troughs in the stable isotope record to identify the potential annual layers (Fig. 4a). Next, this preliminary chronology was compared with the non-sea-salt sulphate ($nssSO_4^{2-} = SO_4^{2-} - 0.25Na^+$) records of the core to identify the well-known volcanic eruption events. The $\delta^{18}O$ measurements were made using a Triple Isotope Water Analyzer (TIWA-45EP, Los Gatos Research), with an external precision of ±0.1‰ (1σ), while ionic concentrations were measured using an ion-exchange chromatograph (Dionex ICS-5000) according to the method detailed by Thamban and others (2010).

Identification of volcanic eruptions with absolute certainty in ice cores from coastal regions is challenging due to the highly variable $nssSO_4^{2-}$ background signals attributed to the presence of a natural background caused by marine biogenic sulphur deposition (Philippe and others, 2016). To separate this natural background, we used the detection threshold method of Sigl and others (2013) using a 100 sample running median (RM) and median absolute deviation (MAD) of the whole record (Fig. 4b). RM and MAD are considered a robust measure of natural background as they are not strongly affected by the presence of outliers, as compared to mean and standard deviation. The detection threshold is thus defined as the sum of RM and three times MAD, and any $nssSO_4^{2-}$ value exceeding this threshold is considered a potential volcanic eruption peak. While multiple values exceeding this threshold were observed in the core, we used only four volcanic marker events that are extensively used in Antarctic ice cores. Accordingly, we identified the $nssSO_4^{2-}$ anomaly peaks related to Pinatubo/Cerro Hudson (1991), El Chichón (1982), Agung (1963) and Cerro Azul (1932) volcanic eruptions in the top 50 m of the ice core (Fig. 4b). Previous studies have shown that the $nssSO_4^{2-}$ records in ice cores can have a

https://doi.org/10.1017/jog.2022.59 Published online by Cambridge University Press

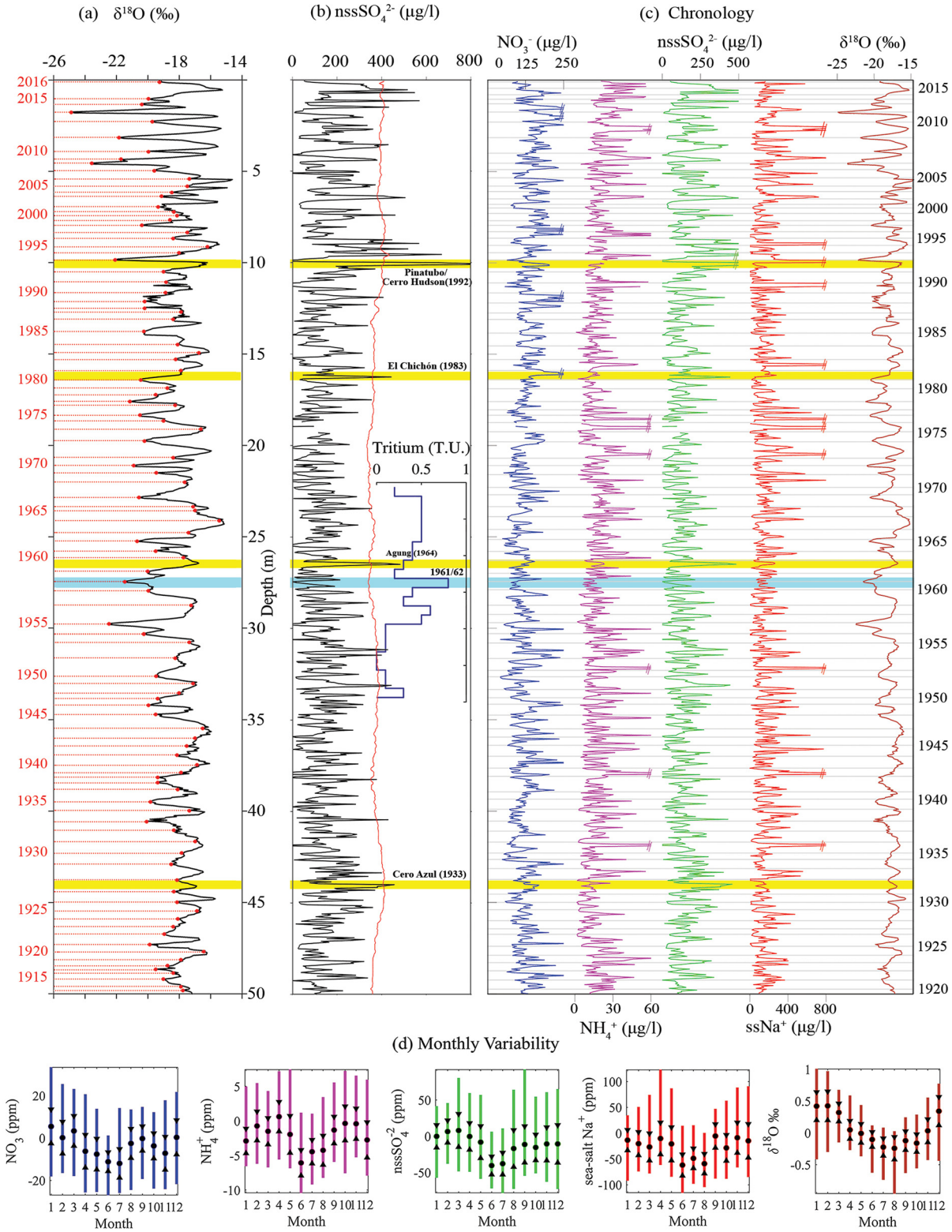

Fig. 4. Establishment of chronology for IND36/9 core using multiple proxies. (a) A preliminary age model using $\delta^{18}O$ records. Annual layers based on the winter minima of the $\delta^{18}O$ record are marked with red dots and red dotted lines. (b) Measured $nssSO_4^{2-}$ records (black) exceeding the detection threshold (red curve) are considered potential volcanic events. Identified volcanic peaks (yellow bands and ages) and the tritium anomaly attributed to the atomic bomb testing of 1961 (blue band) were used as age tie points to constrain the chronology. The final chronology (c) is obtained by annual layer counting, taking into account the seasonal variability in $\delta^{18}O$, $ssNa^+$, $nssSO_4^{2-}$, NO_3^- and NH_4^+. Grey bars represent the annual layers from StratiCounter. Note that the *y*-axes of the chemistry records have been cropped to show maximum variability, and the cropped peaks are marked with breaks to differentiate them from missing data points. (d) Seasonality of chemical proxies and $\delta^{18}O$ for the whole studied section. The black dot shows the median, and the black triangles show the 95% confidence interval of the median. Vertical bars show the interquartile range.

delay of 1–2 years from the time of the volcanic eruption, but this delay may be different for different volcanic events and core locations (Li and others, 2012; Sigl and others, 2013; Emanuelsson and others, 2022). To simplify, we assume a delay of 1 year for all identified volcanic events. To further constrain with an absolute age marker, we measured the tritium concentrations in a

https://doi.org/10.1017/jog.2022.59 Published online by Cambridge University Press

selected 12 m section (inset of Fig. 4b). The tritium profile shows an anomalous peak at 27.25 m depth, coinciding with the well-known tritium anomaly attributed to the atomic bomb testing of Tsar Bomba in 1961 (Cauquoin and others, 2016).

3.2 Multiproxy approach and chronology validation

We used three additional ionic records (ssNa$^+$, NO_3^- and NH_4^+) together with nssSO_4^{2-} and $\delta^{18}O$ records to refine the chronology between the volcanic and tritium tie points (Fig. 4c). Supplementary Figure S1b gives an expanded version of the top 20 m section of the core. A multiproxy approach is needed because the climatic conditions in the coastal Antarctic sites are highly variable, with the snowfall influenced by extreme precipitation events (Turner and others, 2019) and repeated occurrence of summertime melting (Lenaerts and others, 2017), which can disturb the annual signals in $\delta^{18}O$ records. Moreover, firn diffusion can also lead to smoothening of weak annual signals in stable isotope records. We, therefore, used multiple chemical proxy records for annual layer counting to account for the high degree of variability. Winters can be identified with more negative stable isotope values and low concentration of nssSO_4^{2-}, ssNa$^+$, NO_3^- and NH_4^+ and annual layers were marked as concurrent winter troughs.

To ascertain the robustness of the chronology, we used the StratiCounter program (Winstrup and others, 2012) using multiple proxies for the IND36/9 ice core. StratiCounter works on the statistical framework of hidden Markov models and the expectation–maximisation algorithm to automatically recognise annual layers in palaeoclimate archives. It requires training data, and user-defined annual layer counts. We constrained the StratiCounter chronology using volcanic events and the tritium anomaly identified in Figure 4b. Details of the StratiCounter settings are given in Supplementary section S1, and the initial set of manual layer counts used as an input for StratiCounter are shown in Supplementary Figure S1. These manual counts are used to provide a generalised framework. StratiCounter uses this generalised template for annual layers and applies an expectation–maximisation algorithm to continuously update and refine the statistical description of an annual layer, which in turn allows for changes in layer characteristics with depth (Winstrup and others, 2012). To further decrease the dependence of StratiCounter on the initial manual counts, we re-run the program using an improved layer template derived from the algorithm output. Matching the volcanic events and tritium anomaly with the final chronology gives an estimated age error of ±2 years for the past century (Supplementary Table ST1).

We then use this chronology to examine the seasonality of the proxies (Fig. 4d). We calculate anomalies of each month's value from the annual mean value. This is repeated for all the proxies for the period 1919–2016 (Fig. 4d). Since the sampling resolution in the time domain is highly variable and identifying monthly separation in proxy data is debatable, we do not claim monthly resolution, but the median of all monthly values should represent the seasonality of the proxies. We find that the troughs in the $\delta^{18}O$ record typically correspond to the troughs in most chemical species studied here. Although a high degree of variability is observed in the chemical species due to the close proximity of the core site to the open ocean, they are not biannual in nature.

While the accumulation history of the core site is outside the scope of this manuscript, we do observe several anomalously thick and sometimes thin annual layers. This is possibly due to the highly variable precipitation regime of coastal DML, which has been observed to result in anomalous snowfall events, like in 2009, which was recorded using both satellite records (Boening and others, 2012) as well as station-based observations (Gorodetskaya and others, 2013). Regional climate models like RACMO2 also captured this event in their simulations (Lenaerts and others, 2013). A similar degree of variability in snow accumulation record from an ice core has also been observed at a nearby site in the Fimbul Ice Shelf (Kaczmarska and others, 2004), with accumulation rates varying between 0.08 and 0.58 m w.e. during 1737–2000.

3.3 Melt layer quantification and masking

Previous studies have used the melt layer's maximum thickness to calculate the total melt proportion in ice cores (Kaczmarska and others, 2006; Kinnard and others, 2008; Winski and others, 2018). While this method may work well in understanding the temporal variability of annual melt, it is prone to overestimation of the melt proportion. In this study, we used a different approach by manually identifying and masking each melt layer in line scans using a simple algorithm for detecting connected pixels using a prescribed threshold. This image recognition algorithm comprises two primary parts, threshold assignment and pixel connectivity procedure (Fig. 5). First, an adaptive threshold is initially applied to the image by manually assigning a reference point within a melt layer (Fig. 5b). The algorithm then separates the melt layers from the background by considering the empirical distribution of the dark (melt layers) and bright (background) pixels. This results in a binary image (Fig. 5c) of potential melt layers within the core section. Second, since the threshold-based segmentation is not definitive, an eight-neighbourhood pixel connectivity operation is carried out on the binary image. A pixel $P_{i+1,j+1}$ is said to be an eight neighbour of a pixel $P_{i,j}$ if the pixels share either an edge or a vertex, while a region is said to be eight-connected if every pixel in the region can be reached by a combination of moves in the two vertical, two horizontal and four diagonal directions. A mask is created that includes all pixel values that are eight-connected to the reference point and have a grey value within a tolerance range, where tolerance (scalar value) defines the range of pixel values to be included in the mask (grey value of reference point ± tolerance). The tolerance is by default set to 32, but this is adjusted according to each image section, depending on how well the grey values of melt layers are resolved in them. This helps in the identification of any stray pixels segmented during the thresholding process (Fig. 5d). Finally, the holes in the binary mask are flood-filled (Fig. 5e), and the mask is morphologically eroded and then dilated to produce a smooth mask (Fig. 5f). Because the reference point and tolerance were chosen manually, the mask results may vary from iteration to iteration. To ensure accurate results, the melt masks were manually checked against raw images to ensure appropriate masking, and the procedure was repeated (Figs 5b–f) if any differences were identified. The threshold-based connected pixel recognition algorithm ensures that the morphology of the melt layer is well-preserved in the mask and since the VS record has a resolution of 51 µm pixel^{-1}, even melt layers of sub-millimetre-scale would be morphologically well-resolved.

These melt layers appear as clear, dark bands of ice with or without bubbles in VS record. This causes the core section's grey values (pixel intensity) to decrease abruptly, unlike the systematic and smooth changes shown in annual accumulation layers. Our study employed a melt layer mask to exclude the melt section from ice core images while preparing the VS record. This ensures that no bias is introduced in the VS records due to a higher melt in an ice core section. The melt layer mask created for the ice core was used to prepare and quantify the mass proportion of the melted and non-melted segments (Fig. 6a). A melt layer was considered for calculating melt proportion only if it covers at least 50% width of the ice core (Abram and others, 2013).

https://doi.org/10.1017/jog.2022.59 Published online by Cambridge University Press

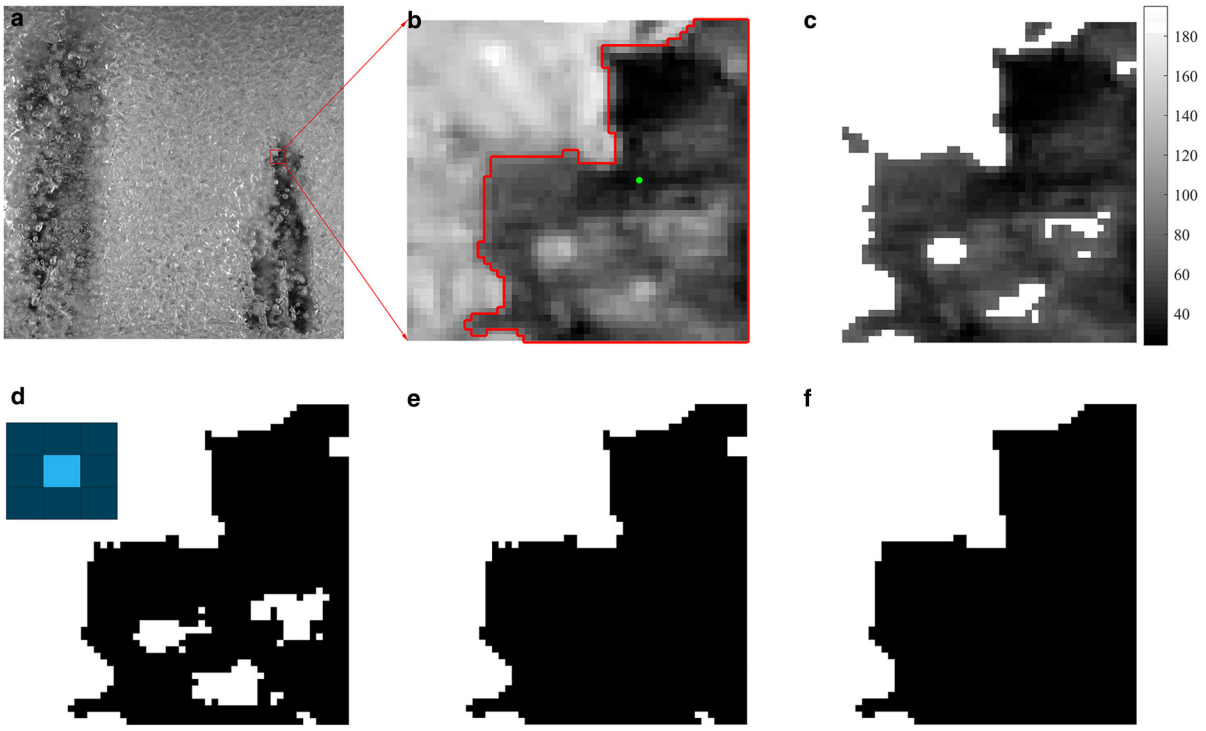

Fig. 5. Melt layer masking with a threshold-based connected pixel algorithm. An ice core section with two visible melts is shown in panel (a), with the red square showing the section zoomed in for detailed reference in the following panels. Panels (b–f) show individual processing steps described in the text. The green dot in panel (b) represents the user input reference point, while the red polygon represents the final mask outline. For this section, a tolerance of 40 is utilised. Inset in panel (d) shows a schematic depiction of an eight-neighbourhood (dark blue) of a pixel (light blue).

The melt proportion is calculated as the percentage of the area of the core section comprised of melt layers by mass (assuming that the melt layer is consistent on the *z*-axis) to each annual layer identified using multi-proxy-based chronology (Fig. 4). The annual proportion of melt in the studied ice core varies between 0 and 4.4%, with a median melt proportion of 0.25% (Fig. 6). We

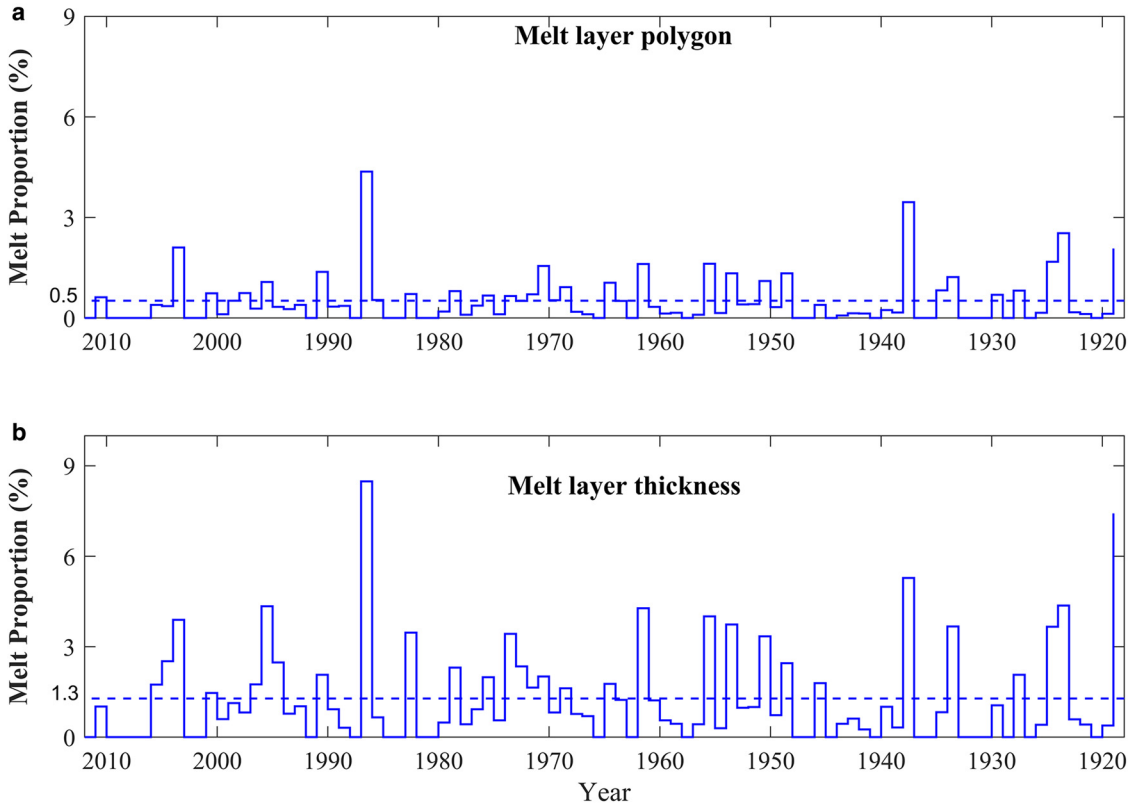

Fig. 6. Melt layer distribution in the ice core was calculated using melt layer polygons (a) and melt layer thickness (b). Estimated annual melt proportion (blue curve) plotted against the age. The blue dashed line shows the mean melt proportion (0.5 and 1.3% by using melt layer polygon and melt layer thickness, respectively) for the time period from 1919 to 2011.

https://doi.org/10.1017/jog.2022.59 Published online by Cambridge University Press

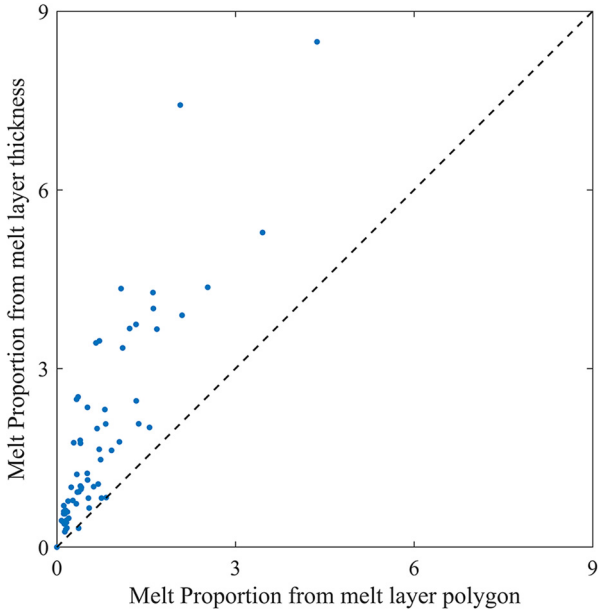

Fig. 7. Scatter plot between annual melt proportion obtained using melt layer polygon and melt layer thickness. The dashed black line is the 1:1 correspondence line. All scatter points are restricted to the left of the black line, showing that melt proportion estimation using layer thickness is overestimated compared to the estimation from melt layer polygons.

define the melt proportion by the area of melt polygons, while other studies use the representative thickness of individual melt layers. This methodological difference may affect the quantification of annual melt proportion. To examine this issue, we also calculated the melt proportion using thickness and compared it with the melt proportion calculated with polygon area (Figs 6, 7). We find that while both methods provide similar temporal change patterns, the melt proportion using layer thickness is overestimated by approximately two times compared to the estimates using melt layer polygons. The higher degree of overestimation generally occurs when the melt layers are not perfectly rectangular in shape or are not consistently well-formed through the width of the core.

Melt layers on polar ice sheets indicate warmer summer air temperatures and are a useful climatic proxy (Kelsey and others, 2010; Winski and others, 2018). Melt layers appear as clear dark patches and are visually closer to ice than firn. These melt layers are primarily perpendicular to the length of the core, and their thickness can vary from less than a millimetre to several centimetres along the width of the core (Fig. 8). Since most melt layers are sub-millimetre to less than a centimetre in width, they do not affect the VS record significantly. However, melt layers with thickness greater than a centimetre or the presence of multiple small melt layers at close intervals can significantly affect the VS record and create the illusion of an annual layer. We thus use the melt mask to remove all melt layer sections from the VS record. Melt frequency and melt percentage are two of the most common metrics for quantifying melt layers, as they are not affected by annual layer thinning (Winski and others, 2018). We used melt percentage to quantify the melt layer record in this core. We suggest that using a melt layer polygon to calculate annual melt proportion instead of melt layer thickness would provide a better estimate of melt history from an ice core.

The occurrence of summertime melting is known to affect the isotopic composition of the near-surface snow. When snow particles come in contact with meltwater, isotopic fractionation occurs at the snow–melt interface. Melting in the early summer affects the highly depleted winter/spring snow, which is present at the surface. The meltwater may also percolate down and refreeze. Although a detailed analysis of the effect of surface melt on the $\delta^{18}O$ record is beyond the scope of the manuscript, the melt features observed in this study are on average 0.5% of the annual layer, with the highest melt proportion being 4.4%. Since the melt proportion at the present core site is low and no percolation of meltwater is observed in the studied section, we conclude that the melt features do not significantly affect the use of stable isotope and chemical profiles from this ice core as a proxy of seasonal cycles. It is also safe to assume that the effect of summertime melting on the snowpack, if any, is restricted to the annual layer.

3.4 Effect of firn density on transmitted light intensity

The intensity of scattered light is maximum near the top, and it gradually decreases to less than half at 50 m depth (Fig. 9a). Firn density gradually increases over this depth range from 420 to ~840 kg m^{-3} (Fig. 9b). The firn density controls this systematic depth trend of the scattered light intensity, as has been previously observed by Sjogren and others (2007) and Kinnard and others (2008). This density effect is removed using circulant single-spectrum analysis (Bógalo and others, 2021). This method works by extracting the underlying signals in a time series by identifying their frequency of oscillation in an automated way by simply introducing the data and a suitable window length. We used the VS record for this purpose and a window length of ten, giving six reconstructed components (RCs). We found that increasing the window length above ten did not significantly affect the outcome and, therefore, proceeded with the same. The first reconstructed component, RC1, replicated this general decreasing trend of VS with depth (Fig. 9a) and has a clear dependence on density (Fig. 9c). We further derived a

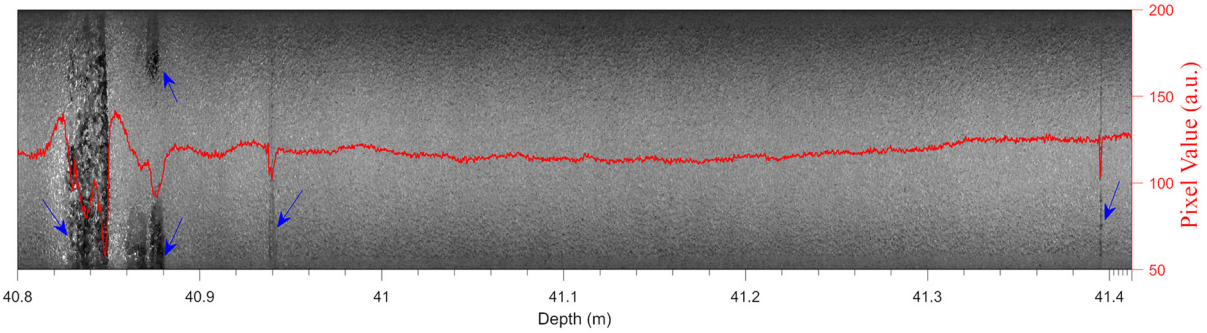

Fig. 8. Line-scan image profile of a core section of 0.65 m long and 7 cm wide. The greyscale (same as Fig. 3) highlights melt layers (marked with blue arrows) of sizes ranging from a few centimetres (first from left) to less than a millimetre (first from right). The mean pixel value along the width of the core is shown (solid red curve). A sharp fall in mean pixel values is observed when melt layers are present, even if less than a millimetre wide.

https://doi.org/10.1017/jog.2022.59 Published online by Cambridge University Press

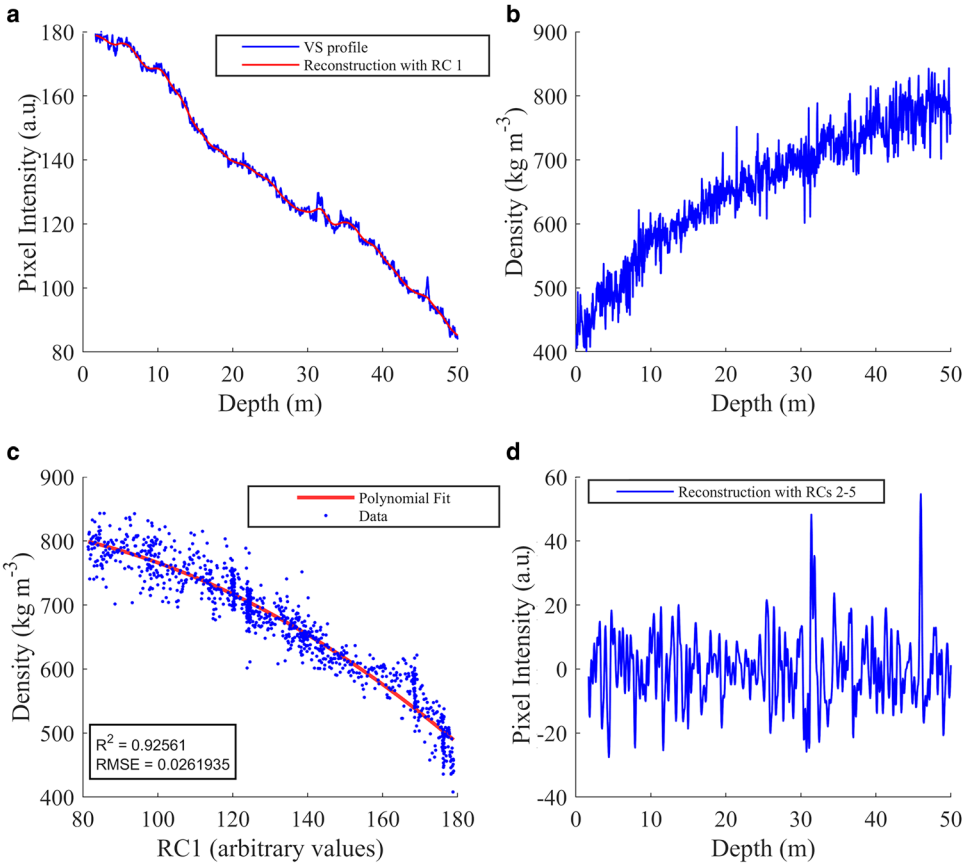

Fig. 9. Depth profiles of the VS record and density. (a) Depth profiles of VS (blue curve) and the RC1 (red curve). (b) Depth profiles of the measured, 5 cm resolution density data (blue). (c) Density dependence of RC1 scattering intensity (blue dots), which is fitted with a second-order polynomial transfer function (solid red curve). (d) The reconstructed seasonal component of VS as a cumulative sum of RC2–RC5.

second-order polynomial transfer function between density and RC1 ($R^2 = 0.92$) (Fig. 9c). The highest order component, RC6, shows largely random noise. Therefore, we consider the sum of the intermediate four components, RC2–RC5, as the representative component of VS variability attributed to the seasonal variability (Fig. 9d).

Variations in several parameters, such as density and micro-inclusions, influence the intensity of light scattered through the ice core section. While density in the firn section has a long-term secular trend (Sjögren and others, 2007), micro-inclusions such as dust and sea-salt inclusions exhibit seasonal variability (Svensson and others, 2005; Winstrup and others, 2012), which may be used to count annual layers. The quantity of air and air–ice contacts in the core substantially impacts the amount of light dispersed by the core. The density of the firn is likewise controlled by its air content; hence, there is a substantial link between density and the intensity of light transmitted through it. A non-linear relationship between the mean pixel intensity and density over the length of the ice cores has also been previously observed by Sjogren and others (2007) and Kinnard and others (2008). We also observe a similar non-linear relationship and find that once the trend due to the gradual increase in density is separated from the VS record, the resultant component would possibly represent the seasonal variability and can be used for annual layer counting.

3.5 VS from line-scan images as a tool for firn core chronology

To examine the potential of high-resolution VS records as a reliable tool for annual layer counting in coastal Antarctica, we first construct an age–depth model based on layer counting of the VS record and then compared the age model against the nssSO_4^{2-} profile that has volcanic events and tritium marker horizons demarcated (Fig. 10). Winters can be identified as peaks in the VS record. The processed VS record has relatively less noise, but ambiguous peaks and shoulders are still present. If all such ambiguous peaks and shoulders are identified as annual layers, it can result in significant overcounting. To ascertain the robustness of the VS age–depth model, we used StratiCounter for annual layer identification in the VS record. An initial annual layer template is provided for the algorithm, with certain and uncertain layers marked and constrained using the time markers identified in Section 3.1. The input layer template and StratiCounter annual layer outputs are shown in Supplementary Figures S2 and S3. We find that the age–depth model from VS is highly robust, with the error in the chronology being <±2 years for the past century (Supplementary Table ST1).

The seasonality of the VS record is calculated as explained in Section 3.2 and shown in Figure 10c. The reported age model error for the majority of high-accumulation ice core records from coastal Antarctica for the past century is ±2 years or greater (Isaksson and others, 1999; Thamban and others, 2006; Naik and others, 2010; Thamban and others, 2013; Laluraj and others, 2014; Philippe and others, 2016). Therefore, the high-resolution VS profile studied here provides a reliable means to constrain the ice core chronology with similar accuracy to previous studies. Our study shows that VS profiles have high potential as a preliminary and supplemental age tool due to their clear seasonality (Fig. 10c), especially considering that analysis of isotopic and chemical proxies requires more time and resources. Considering the extensive summertime melting in low-elevation sites of coastal Antarctica, where annual layer counting and chronological constraints using stable isotope and chemical records are susceptible

https://doi.org/10.1017/jog.2022.59 Published online by Cambridge University Press

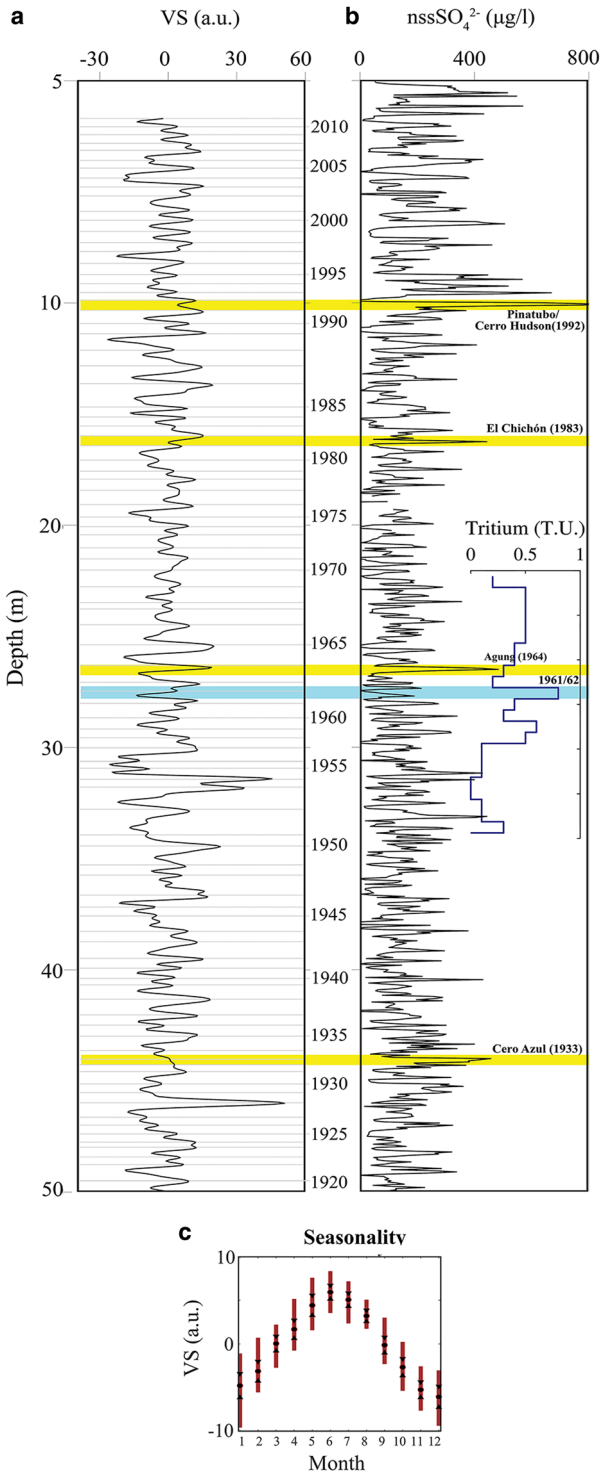

Fig. 10. Comparison of age models using VS record and volcanic events. (a) Depth profile of VS (sum of the RC2–RC5). Annual layers (winter peaks) using the StratiCounter program are marked with grey bars, and every fifth year is labelled. (b) Same as Figure 4b. (c) Seasonality plot of VS record plotted similar to Figure 4d. Note that the VS record uses arbitrary units (a.u.).

to larger uncertainties, the VS method would be advantageous when used in tandem with other proxies.

The ultra-high-resolution VS profile of the ice core also provides a detailed picture of the physical processes and environmental variability during the period. Throughout the length of the core, clear ice core layering is visible. The dark and bright horizons observed in the VS profiles are formed due to variation in micro-inclusions in the ice cores, and these micro-inclusions are known to have seasonal variations (Winstrup and others, 2012). However, in the top snow/firn section of the ice core, where annual layer thickness is large, the high resolution of VS data makes it challenging to differentiate annual signals from the noise. However, with proper filtering and downsampling, it is possible to extract the annual signals from the VS profile. VS in ice cores can be challenging due to non-uniform firnification or depositional events and becomes less clear with increasing age and depth, owing to densification and other physical changes. Thus, identification of annual layers solely based on VS can be tricky due to the presence of multiple peaks within an annual layer; however, when several of the above methods are combined, such discrepancies can be identified and removed. Hence, VS provides valuable support in identifying seasonal cycles with higher confidence, resulting in a more robust chronology.

4. Conclusions

Our study demonstrated that VS records reconstructed using line-scan images from the firn section of an ice core can be successfully used to establish an independent high-resolution age–depth model. Traditional methods of annual layer counting using stable isotope and major ion chemistry records are laborious, potentially susceptible to artefacts related to summertime melting and harder to interpret for annual layer counting in the coastal region due to the close proximity to the oceanic processes and the influence of storm activities. VS profiles are proposed as an important supplemental dating tool in coastal regions of Antarctica. Also, VS profiles can be used to develop a preliminary chronology in a short analysis time, while the other chemical and isotope methods require more time and resources to acquire. The VS profile of the firn section of the ice core is dominantly affected by the temporal changes in density, but automated signal extraction procedures can separate it to distil the seasonal signals attributed to the dust and sea-salt inclusions. The line-scan images can also be used to identify and quantify the melt layers routinely noticed in ice cores from low-elevation sites of Antarctica. Such melt layers can be appropriately masked during the pre-processing of the line-scan images, enabling us to reconstruct the chronology of ice cores from coastal Antarctica. We demonstrate that quantifying annual melt proportion using only the thickness of the melt layer can lead to overestimations and propose using the melt layer polygon area for calculating annual melt proportions. The reconstructed VS profile of the top 50 m section of an ice core from coastal DML revealed an excellent match with the chronology of the ice core based on a multi-proxy approach, supported with independent age markers of volcanic events and tritium anomaly, with the highest error being ±2 years for the past century. We conclude that ultra-high-resolution VS records from coastal Antarctica could be valuable in reconstructing the chronology of ice cores.

Supplementary material. To view supplementary material for this article, please visit https://doi.org/10.1017/jog.2022.59

Data. The IND36/9 ice core records of $\delta^{18}O$, $nssSO_4^{2-}$, $ssNa^+$, NO_3^-, NH_4^+ and VS are available at National Polar Data Centre (http://ramadda.npdc.ncpor.res.in:8080/repository/entry/show?entryid=ea609882–3911).

Acknowledgements. Ice core drilling and field expedition have been made successful with the support of the NCPOR logistics leaders, Maitri logistics team and NPI logistic personnel. Ashish Paigankar and Tariq Ejaz are acknowledged for their contributions to ice core processing and chemical analysis. RD acknowledges University Grant Commission for a research fellowship grant and Prof. Kotha Mahender (Goa University) for valuable guidance. We thank the scientific editor Mathieu Casado and two anonymous reviewers for constructive comments and helpful suggestions, which have improved the manuscript. This is NCPOR contribution number J-17/2022-23.

Author contributions. MT and RD defined the study objectives. MT, CML, KM and BLR collected the ice core. RD led the ice core processing, line scanning and analysis with support from BLR, KM and CML. RD analysed and interpreted the data with contributions from MT and KeM. All authors contributed to the manuscript. MT and KeM were the project leaders.

Financial support. This research has been supported by the Ministry of Earth Sciences, India (grant no. MoES/Indo-Nor/PS-3/2015) and the Research Council of Norway (grant no. 248780) for the joint India–Norway project, 'Mass balance, dynamics, and climate of the central Dronning Maud Land coast, East Antarctica' (MADICE).

Code availability. The MATLAB codes, used for (i) pre-processing of line-scan images and (ii) quantification of melt proportion, are available on the GitHub page of Rahul Dey (www.github.com/dey-rahul).

References

Abram NJ and 8 others (2013) Acceleration of snow melt in an Antarctic Peninsula ice core during the twentieth century. *Nature Geoscience* **6**(5), 404–411. doi: 10.1038/Ngeo1787

Alley RB and 11 others (1997) Visual-stratigraphic dating of the GISP2 ice core: basis, reproducibility, and application. *Journal of Geophysical Research: Oceans*, **102**(C12), 26367–26381. doi: 10.1029/96jc03837

Boening C, Lebsock M, Landerer F and Stephens G (2012) Snowfall-driven mass change on the east Antarctic ice sheet. *Geophysical Research Letters* **39** (21), L21501. doi: 10.1029/2012gl053316

Bógalo J, Poncela P and Senra E (2021) Circulant singular spectrum analysis: a new automated procedure for signal extraction. *Signal Processing* **179**, 107824. doi: 10.1016/j.sigpro.2020.107824

Cauquoin A, Jean-Baptiste P, Risi C, Fourré É and Landais A (2016) Modeling the global bomb tritium transient signal with the AGCM LMDZ-iso: a method to evaluate aspects of the hydrological cycle. *Journal of Geophysical Research: Atmosphere* **121**(21), 12,612–12,629. doi: 10.1002/2016JD025484

Das SB and Alley RB (2005) Characterization and formation of melt layers in polar snow: observations and experiments from west Antarctica. *Journal of Glaciology* **51**(173), 307–312. doi: 10.3189/172756505781829395

Drews R and 5 others (2015) Evolution of Derwael ice rise in Dronning Maud Land, Antarctica, over the last millennia. *Journal of Geophysical Research-Earth Surface* **120**(3), 564–579. doi: 10.1002/2014jf003246

Ejaz T, Rahaman W, Laluraj CM, Mahalinganathan K and Thamban M (2021) Sea ice variability and trends in the western Indian ocean sector of Antarctica during the past two centuries and its response to climatic modes. *Journal of Geophysical Research: Atmospheres* **126**, e2020JD033943. doi: 10.1029/2020JD033943

Emanuelsson BD, Thomas ER, Tetzner DR, Humby JD and Vladimirova DO (2022) Ice core chronologies from the Antarctic Peninsula: the Palmer, Jurassic, and Rendezvous Age-scales. *Geosciences* **12**(2), 87. doi: 10.3390/geosciences12020087

Goel V, Brown J and Matsuoka K (2017) Glaciological settings and recent mass balance of Blåskimen Island in Dronning Maud Land, Antarctica. *The Cryosphere* **11**(6), 2883–2896. doi: 10.5194/tc-11-2883-2017

Goel V and 5 others (2020) Characteristics of ice rises and ice rumples in Dronning Maud Land and Enderby Land, Antarctica. *Journal of Glaciology* **66**(260), 1064–1078. doi: 10.1017/jog.2020.77

Gorodetskaya IV and 5 others (2013) Meteorological regimes and accumulation patterns at Utsteinen, Dronning Maud Land, East Antarctica: analysis of two contrasting years. *Journal of Geophysical Research: Atmospheres* **118** (4), 1700–1715. doi: 10.1002/jgrd.50177

Goursaud S and 10 others (2017) A 60-year ice-core record of regional climate from Adélie Land, coastal Antarctica. *The Cryosphere* **11**(1), 343–362. doi: 10.5194/tc-11-343-2017

Howat IM, Porter C, Smith BE, Noh MJ and Morin P (2019) The reference elevation model of Antarctica. *The Cryosphere* **13**(2), 665–674. doi: 10.5194/tc-13-665-2019

Isaksson E and 5 others (1999) Accumulation and proxy-temperature variability in Dronning Maud Land, Antarctica, determined from shallow firn cores. *Annals of Glaciology* **29**, 17–22. doi: 10.3189/172756499781821445

Johnsen S (1977) Stable isotope homogenization of polar firn and ice. International Symposium on Isotopes and Impurities in Snow and Ice, Grenoble, 28–30 August 1975; International Association of Hydrological Sciences, Publication No. 118, pp. 210–219.

Kaczmarska M and 10 others (2004) Accumulation variability derived from an ice core from coastal Dronning Maud Land, Antarctica. *Annals of Glaciology* **39**, 339–345. doi: 10.3189/172756404781814186

Kaczmarska M and 7 others (2006) Ice core melt features in relation to Antarctic coastal climate. *Antarctic Science* **18**(2), 271–278. doi: 10.1017/S0954102006000319

Kameda T and 5 others (1995) Melt features in ice cores from Site J, southern Greenland: some implications for summer climate since AD 1550. *Annals of Glaciology* **21**, 51–58. doi: 10.3189/S0260305500015597

Kelsey E, Wake C, Kreutz K and Osterberg E (2010) Ice layers as an indicator of summer warmth and atmospheric blocking in Alaska. *Journal of Glaciology* **56**, 715–722. doi: 10.3189/002214310793146214

Kinnard C and 7 others (2008) Stratigraphic analysis of an ice core from the Prince of Wales Icefield, Ellesmere Island, Arctic Canada, using digital image analysis: high-resolution density, past summer warmth reconstruction, and melt effect on ice core solid conductivity. *Journal of Geophysical Research* **113**(D24), D24120. doi: 10.1029/2008jd011083

Krinner G, Magand O, Simmonds I, Genthon C and Dufresne JL (2007) Simulated Antarctic precipitation and surface mass balance at the end of the twentieth and twenty-first centuries. *Climate Dynamics* **28**(2), 215–230. doi: 10.1007/s00382-006-0177-x

Krischke A, Oechsner U and Kipfstuhl S (2015) Rapid microstructure analysis of polar ice cores. *Optik & Photonik* **10**(2), 32–35. doi: 10.1002/opph.201500016

Laluraj CM, Thamban M and Satheesan K (2014) Dust and associated geochemical fluxes in a firn core from coastal East Antarctica and its linkages with southern hemisphere climate variability over the last 50 years. *Atmospheric Environment* **90**, 23–32. doi: 10.1016/j.atmosenv.2014.03.031

Laluraj CM, Rahaman W, Thamban M and Srivastava R (2020) Enhanced dust influx to south Atlantic sector of Antarctica during the late-20th century: causes and contribution to radiative forcing. *Journal of Geophysical Research: Atmospheres* **125**(8), e2019JD030675. doi: 10.1029/2019jd030675

Legrand M and Mayewski P (1997) Glaciochemistry of polar ice cores: a review. *Reviews of Geophysics* **35**(3), 219–243. doi: 10.1029/96rg03527

Lenaerts JTM and 6 others (2013) Recent snowfall anomalies in Dronning Maud Land, East Antarctica, in a historical and future climate perspective. *Geophysical Research Letters* **40**(11), 2684–2688. doi: 10.1002/grl.50559

Lenaerts JTM and 11 others (2014) High variability of climate and surface mass balance induced by Antarctic ice rises. *Journal of Glaciology* **60** (224), 1101–1110. doi: 10.3189/2014JoG14J040

Lenaerts JTM and 12 others (2017) Meltwater produced by wind–albedo interaction stored in an East Antarctic ice shelf. *Nature Climate Change* **7** (1), 58–62. doi: 10.1038/nclimate3180

Li R, Xiao C, Sneed S and Yan MJAS (2012) A continuous 293-year record of volcanic events in an ice core from Lambert Glacier Basin, East Antarctica. *Antarctic Science* **24**(3), 293–298. doi: 10.1017/S0954102011000897

Magudeeswaran V and Singh JF (2017) Contrast limited fuzzy adaptive histogram equalization for enhancement of brain images. *International Journal of Imaging Systems and Technology* **27**(1), 98–103. doi: 10.1002/ima.22214

Matsuoka K and 19 others (2015) Antarctic ice rises and rumples: their properties and significance for ice-sheet dynamics and evolution. *Earth-Science Reviews* **150**, 724–745. doi: 10.1016/j.earscirev.2015.09.004

Matsuoka K and 21 others (2021) Quantarctica, an integrated mapping environment for Antarctica, the Southern Ocean, and sub-Antarctic islands. *Environmental Modelling & Software* **140**, 105015. doi: 10.116/j.envsoft.2021.105015

McGwire KC and 6 others (2008) Dating annual layers of a shallow Antarctic ice core with an optical scanner. *Journal of Glaciology* **54**(188), 831–838. doi: 10.3189/002214308787780021

Morcillo G, Faria SH and Kipfstuhl S (2020) Unravelling Antarctica's past through the stratigraphy of a deep ice core: an image-analysis study of the EPICA-DML line-scan images. *Quaternary International* **566–567**, 6–15. doi: 10.1016/j.quaint.2020.07.011

Mouginot J, Scheuchl B and Rignot E (2017) MEaSUREs Antarctic Boundaries for IPY 2007–2009 from Satellite Radar, Version 2. GroundingLine_Antarctica_v02. *Boulder, Colorado USA. NASA National Snow and Ice Data Center Distributed Active Archive Center*. doi: 10.5067/AXE4121732AD

https://doi.org/10.1017/jog.2022.59 Published online by Cambridge University Press

Naik SS, Thamban M, Laluraj CM, Redkar BL and Chaturvedi A (2010) A century of climate variability in central Dronning Maud Land, East Antarctica, and its relation to southern annular mode and El Niño-Southern oscillation. *Journal of Geophysical Research* **115**(D16), D16102. doi: 10.1029/2009jd013268

Philippe M and 10 others (2016) Ice core evidence for a 20th century increase in surface mass balance in coastal Dronning Maud Land, East Antarctica. *The Cryosphere* **10**(5), 2501–2516. doi: 10.5194/tc-10-2501-2016

Pohjola VA and 7 others (2002) Effect of periodic melting on geochemical and isotopic signals in an ice core from Lomonosovfonna, Svalbard. *Journal of Geophysical Research: Atmospheres* **107**(D4), 4036. doi: 10.1029/2000jd000149

Pratap B and others (2021) Three-decade spatial patterns in surface mass balance of the Nivlisen Ice Shelf, central Dronning Maud Land, East Antarctica. *Journal of Glaciology* **68**(267), 174–186. doi: 10.1017/jog.2021.93

Rignot E and 5 others (2019) Four decades of Antarctic ice sheet mass balance from 1979–2017. *Proceedings of the National Academy of Sciences* **116**(4), 1095. doi: 10.1073/pnas.1812883116

Sigl M and 11 others (2013) A new bipolar ice core record of volcanism from WAIS divide and NEEM and implications for climate forcing of the last 2000 years. *Journal of Geophysical Research: Atmospheres* **118**(3), 1151–1169. doi: 10.1029/2012jd018603

Sinclair KE, Bertler NAN and Trompetter WJ (2010) Synoptic controls on precipitation pathways and snow delivery to high-accumulation ice core sites in the Ross Sea region, Antarctica. *Journal of Geophysical Research* **115**, D22112. doi: 10.1029/2010jd014383

Sjogren B and 6 others (2007) Instruments and methods – determination of firn density in ice cores using image analysis. *Journal of Glaciology* **53**(182), 413–419. doi: 10.3189/002214307783258369

Stenni B and 8 others (1999) 200 years of isotope and chemical records in a firn core from Hercules Névé, Northern Victoria Land, Antarctica. *Annals of Glaciology* **29**, 106–112. doi: 10.3189/172756499781821175

Stenni B and 6 others (2000) Snow accumulation rates in northern Victoria Land, Antarctica, by firn-core analysis. *Journal of Glaciology* **46**(155), 541–552. doi: 10.3189/172756500781832774

Svensson A and 7 others (2005) Visual stratigraphy of the north Greenland ice core project (NorthGRIP) ice core during the last glacial period. *Journal of Geophysical Research-Atmospheres* **110**(D2), D02108. doi: 10.1029/2004jd005134

Svensson A and 13 others (2008) A 60 000 year Greenland stratigraphic ice core chronology. *Climate of the Past* **4**(1), 47–57. doi: 10.5194/cp-4-47-2008

Takata M and 5 others (2004) Stratigraphic analysis of Dome Fuji Antarctic ice core using an optical scanner. *Annals of Glaciology* **39**, 467–472. doi: 10.3189/172756404781813899

Tedesco M and Monaghan AJ (2009) An updated Antarctic melt record through 2009 and its linkages to high-latitude and tropical climate variability. *Geophysical Research Letters* **36**, L18502. doi: 10.1029/2009GL039186

Thamban M and 7 others (2006) Aerosol perturbations related to volcanic eruptions during the past few centuries as recorded in an ice core from the central Dronning Maud Land, Antarctica. *Current Science* **91**(9), 1200–1207.

Thamban M and 5 others (2010) Glaciochemistry of surface snow from the Ingrid Christensen Coast, East Antarctica, and its environmental implications. *Antarctic Science* **22**(4), 435–441. doi: 10.1017/s0954102010000155

Thamban M, Naik SS, Laluraj CM, Chaturvedi A and Ravindra R (2013) Antarctic climate variability during the past few centuries based on ice core records from coastal Dronning Maud Land and its implications on the recent warming. In Sinha R and Ravindra R (eds), *Earth System Processes and Disaster Management*. Berlin, Heidelberg: Springer Berlin Heidelberg, pp. 51–66. doi: 10.1007/978-3-642-28845-6_5

Thamban M, Rahaman W and Laluraj C (2020) Millennial to quasi-decadal variability in Antarctic climate system as evidenced from high-resolution ice core records. *Current Science* **119**(2), 255–264.

Turner J and 12 others (2019) The dominant role of extreme precipitation events in Antarctic snowfall variability. *Geophysical Research Letters* **46**(6), 3502–3511. doi: 10.1029/2018GL081517

van den Broeke M (2005) Strong surface melting preceded collapse of Antarctic Peninsula ice shelf. *Geophysical Research Letters* **32**(12), L12815. doi: 10.1029/2005GL023247

Winski D and 10 others (2018) A 400-year ice core melt layer record of summertime warming in the Alaska Range. *Journal of Geophysical Research: Atmospheres* **123**(7), 3594–3611. doi: 10.1002/2017jd027539

Winstrup M and 10 others (2012) An automated approach for annual layer counting in ice cores. *Climate of the Past* **8**(6), 1881–1895. doi: 10.5194/cp-8-1881-2012

Zhang M and 6 others (2006) 250 years of accumulation, oxygen isotope and chemical records in a firn core from Princess Elizabeth Land, East Antarctica. *Journal of Geographical Sciences* **16**(1), 23–33. doi: 10.1007/s11442-006-0103-5

https://doi.org/10.1017/jog.2022.59 Published online by Cambridge University Press